Mechanical Systems and Signal Processing 123 (2019) 117–130

Contents lists available at ScienceDirect

Mechanical Systems and Signal Processing

journal homepage: www.elsevier.com/locate/ymssp

Tunable and reconfigurable mechanical transmission-line metamaterials via direct active feedback control ☆

Lea Sirota [a,*], Fabio Semperlotti [b], Anuradha M. Annaswamy [a]

[a] Department of Mechanical Engineering, MIT, Cambridge, MA 02139, USA
[b] Ray W. Herrick Laboratories, School of Mechanical Engineering, Purdue University, West Lafayette, IN 47907, USA

ARTICLE INFO

Article history:
Received 9 September 2018
Received in revised form 31 December 2018
Accepted 2 January 2019
Available online 11 January 2019

Keywords:
Wave propagation
Wave suppression
Active mechanical metamaterials

ABSTRACT

We consider the problem of using active feedback control to create tunable and reconfigurable mechanical metamaterials capable of supporting unconventional wave propagation mechanisms. The nominal system chosen for this analysis is a one-dimensional homogeneous bar having periodically distributed force actuators and subject to longitudinal waves. We note that this system does not make use of local inclusions, instead the actuators are attached directly to the beam and achieve metamaterial properties by means of periodically applied forces. We design control algorithms in order to achieve desired constitutive parameters for the metamaterial in closed loop. In particular, the control system is designed to generate either zero or negative values of the effective properties (i.e. stiffness and mass) to obtain a metamaterial with different dynamic behaviors. Four different regimes of effective properties are considered in this study: single negative or zero, double negative, double zero, double positive. The constitutive parameters achievable via the direct control approach are therefore defined only by the feedback algorithms and are not confined to any particular properties that would otherwise be imposed by local resonators. We model and analyze the system by fractional order transfer functions, which explicitly exhibit the special characteristics of the metamaterial, including the constitutive parameters, dispersion, and transmission and reflection properties. We illustrate the stability and performance of the control system through numerical simulations. Finally we note that, despite the choice of the mechanical system used in this study, the proposed results have general applicability to all those systems described by the second order wave equation in their nominal uncontrolled state.

1. Introduction

Metamaterials are artificially designed structures, usually of periodic nature, that can exhibit properties not necessarily available in natural materials, such as negative or zero effective constitutive parameters. The original concept was formulated for electro-magnetic systems [1–4], and later extended to acoustic and elastic systems. A variety of unconventional wave propagation effects have been proposed over the years including Dirac-like cone dispersion [5], acoustic leaky wave antennas [6], subwavelength imaging [7], cloaking [8], and many more as summarized in [9]. The current work aims at

☆ This paper was not presented at any IFAC meeting.

* Corresponding author.
E-mail addresses: lbeilkin@mit.edu (L. Sirota), fsemperl@purdue.edu (F. Semperlotti), aanna@mit.edu (A.M. Annaswamy).

https://doi.org/10.1016/j.ymssp.2019.01.001
0888-3270/

developing transmission line type metamaterials, which essentially represent one-dimensional periodic waveguide. Such metamaterial waveguides were described in [10–12] for electric transmission lines involving periodic arrangements of capacitors, resistors, and inductors. Later, the analogous concept of acoustic waveguides were reported in [13–17] where local acoustic resonators and scatterers were periodically distributed along a tube. Closely related to these acoustic systems are mechanical metamaterial waveguides that have been reported in [18–20] based on either discrete or continuous configurations [21].

To date, most of the acoustic and elastic metamaterial research has considered passive structures where the unit cell is made of passive materials having given shape and dimensions. Such material system results in constant dynamic properties (i.e. effective parameters and dispersion) at a given operating frequency. In an attempt to achieve tunable properties and extended operating ranges, active materials [22–26] have been considered. In the existing literature, active metamaterials have been implemented via actuators connected to built-in passive resonators in an effort to tune the response of locally resonant units. As an example, in [22] piezoelectric disks were installed into cavities to control the dynamic stiffness of the acoustic unit cell and design tunable metasurfaces. In [23], programmable effective acoustic mass density of a single unit cell was obtained using active membranes attached to a tube section, whereas in [24] an active membrane was attached to the bottom of a passive resonating cavity to control the effective acoustic modulus. In [25], piezoelectric patches attached to a beam with periodic protrusions were used to tune the bending stiffness of the beam. In [26], velocity and acceleration feedback control was designed for a discrete chain of mass-in-mass passive resonators in order to tune the stop band of the resulting negative effective mass metamaterial. The advantage of this class of active metamaterials consists in the fact that the basic properties of the underlying passive structure can be tuned to different frequencies (within the available actuators magnitude and bandwidth), hence extending the operating dynamic range of the metamaterial. One the other side, however, the achievable effective constitutive parameters are limited in the neighborhood of the properties set for the passive resonators. Another disadvantage is the manufacturing complexity of locally resonant inclusions that are still required in currently available active designs.

The goal of this work is to design an active mechanical metamaterial implemented only via external actuation, i.e. by using a periodic distribution of actuators attached to the host structure and activated by a proper control logic. Such design will leave the properties of the host structure unchanged when the transducers are inactive, while it will produce desired combinations of dynamic constitutive parameters when using a properly designed feedback control. It appears that this approach could lead to real-time tunable and reconfigurable metamaterial configurations. In the following, we will show how the host structure can be turned into four different dynamic systems operating at the same frequency by proper actuation of the controller. This approach could also turn any conventional material into a metamaterial and, potentially, it could be retrofitted to existing systems. For the nominal system, we consider a beam in axial vibration. This system, when uncontrolled, is governed by a second order wave equation and will allow extension of the results to analogous systems such as, for example, acoustic ducts and electric transmission-lines. The nominal system is augmented by active elements operating in a real time loop and controlled by a feedback logic capable of targeting desired effective constitutive parameters (e.g. equivalent effective mass and stiffness).

The control system is designed using infinite dimension transfer function modeling. This kind of modeling was reported in the literature for vibrating strings and beams, and acoustic ducts [27,28], rotating shafts [29,30], vibrating membranes [31], power grid swing dynamics, [32,33] among other systems. For linear systems, the transfer function model can capture the exact wave propagation properties of the structure, including the dynamic constitutive parameters, the dispersion relation, time delays and reflection/transmission coefficients. We derive the model for the nominal conventional beam and for the target metamaterial on the section of the beam were actuators are applied. This model, which turns out to be of fractional order, is the key element in the control design.

The paper is organized as follows. In Section 2, we present the feedback control setup on top of the conventional beam, derive the transfer function models for the nominal and the target systems and discuss their properties. Then, we design the control algorithm capable of generating an equivalent mechanical metamaterial having prescribed effective constitutive parameters. In Section 3, we consider an example of particular constitutive parameters, that are similar to those reported in the literature for acoustic and electric metamaterials. In Section 4, we present numerical simulations of the control system performance. In Section 5 we conclude the paper and in Appendix A we present the closed loop stability analysis.

2. Mechanical metamaterial modeling and control

We consider the problem of creating a mechanical metamaterial using active control elements that are periodically distributed along an otherwise homogeneous mechanical structure and that operate in a real time feedback loop. In Section 2.1 we discuss the proposed metamaterial setup while in Section 2.2 we derive the transfer function model of the target closed loop system.

2.1. Description of the system

The proposed setup is schematically illustrated in Fig. 1. It consists of a conventional homogeneous beam of length L and cross-section A as well as constant and positive mass density and stiffness (Young modulus), denoted here by the pair

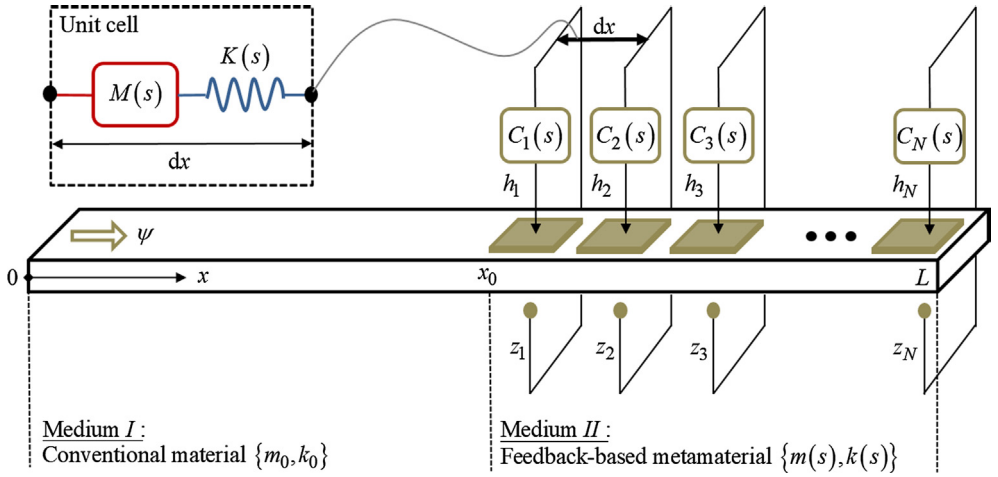

Fig. 1. A schematic diagram of a mechanical active metamaterial generated by feedback control. The base system is a conventional homogeneous beam of length L and cross-section A, characterized by positive values of the static constitutive parameters, which are the mass density m_0 and stiffness (Young modulus) k_0. A force source ψ drives the system at $x = 0$. At the section $x_0 \leqslant x \leqslant L$, active elements (gold flat squares) are assumed attached to the beam on both sides with equal spacing of dx from x_0 to L. The elements are actuated simultaneously, thereby exciting only the longitudinal modes of the beam. The active elements operate in feedback loops according to the controllers $C_j(s)$. We denote the uncontrolled section $0 \leqslant x < x_0$ by medium I, the controlled section $x_0 \leqslant x \leqslant L$ by medium II, the control inputs by h_j and the measurements by z_j. For brevity, unity actuators dynamics is assumed. The actuators allocation renders medium II a periodic structure with unit cell length of dx. At the j unit cell (dashed box), the control law $h_j = -C_j(s)z_j$ generates an effective stiffness $K(s) = k(s)/\mathrm{d}x$ and effective mass $M(s) = m(s)\mathrm{d}x$.

$\{m_0, k_0\}$. A concentrated force ψ is applied at $x = 0$ on the neutral plane and oriented along the x axis so to excite only longitudinal waves. The beam can be decomposed into two sections. The first section, $0 \leqslant x < x_0$, does not have external actuators (hence it is not actively controlled) and is denoted by medium I. The second section, $x_0 \leqslant x < L$, consists of the active metamaterial section and it is denoted by medium II. This section comprises actuators, e.g. piezoelectric or microfiber composite (MFC) patches schematically indicated by gold flat squares, that are connected to the beam and periodically distributed with a fixed spacing dx from x_0 to L. The spacing dx defines the unit cell length. We stress out that since no passive resonating elements are present in the setup, the metamaterial fabrication is substantially simplified, as it comprises attaching commercially available actuators to a conventional homogeneous bar. The actuators are assumed attached on both sides of the beam and actuated simultaneously so to excite only the longitudinal modes of the beam. The actuators operate in real time feedback loops with controllers $C_j(s)$. The goal of this work is to design control laws for $C_j(s)$ so that, in closed loop, medium II will exhibit a target dynamic mass and stiffness $\{m(s), k(s)\}$, where $m(s) = m_0\widetilde{M}(s)$ and $k(s) = k_0\widetilde{K}(s)$. We denote the system $\{m(s), k(s)\}$ as the target system.

Ideally, the choice of $\widetilde{M}(s)$ and $\widetilde{K}(s)$ is completely free and can potentially achieve any value. This is a direct consequence of our approach that does not rely on the existence of local inclusions between the actuators and the host structure. As previously mentioned, these inclusions would otherwise impose constraints on the achievable dynamic constitutive parameters. Although our control design is for the effective continuous system, the actual actuation is discrete. At the cell j, the control input is denoted by h_j and the respective measurement by z_j. For each cell, the controller generates the effective mass $M(s) = M_0\widetilde{M}(s)$ and stiffness $K(s) = K_0\widetilde{K}(s)$, where $M_0 = m_0\mathrm{d}x$ and $K_0 = k_0/\mathrm{d}x$ are the undriven nominal unit cell mass and stiffness. $m(s)$ and $k(s)$ are therefore the continuous limits of $M(s)$ and $K(s)$. When undriven ($h_j = 0$), we retrieve $\widetilde{M}(s) = 1$ and $\widetilde{K}(s) = 1$.

2.2. Transfer function model derivation

In this section we derive the transfer function models for the conventional medium I and the metamaterial medium II, as obtained in closed loop. To facilitate the analysis of the system and the results that will follow, we eliminate any wave reflections from the boundaries $x = 0$ and $x = L$ by assuming that impedance matching controllers are operating at the boundaries. Under ideal conditions, such controllers can eliminate completely boundary reflections.

2.2.1. Modeling the conventional medium I

The displacement of the conventional medium I and the internal force reaction, respectively denoted by y^I and f, satisfy the constitutive equations, i.e. Hooke's law and conservation of momentum, which in the Laplace domain are given by

$$f(x;s) = Ak_0 y^I_x(x;s), \tag{1a}$$

$$f_x(x;s) = Am_0 s^2 y^I(x;s), \tag{1b}$$

where A, m_0 and k_0 are the cross-section, mass density and stiffness of the beam, s is the Laplace variable, and the subindex x indicates the derivative with respect to the spatial variable. The combination of (1a) with (1b) implies that medium I is governed by the classic wave equation [34], which in the Laplace domain is expressed as

$$y^I_{xx}(x;s) = \frac{s^2}{c^2} y^I(x;s), \tag{2}$$

where $c = \sqrt{k_0/m_0}$ is the longitudinal wave speed. At the boundary $x = 0$, in addition to the source ψ, we employ an impedance matching controller to eliminate reflections from $x = 0$. We follow the results reported in [29], where it was shown that the controller has the form of an active damper, whose value must be set to the characteristic impedance z_0 of medium I, given by

$$z_0 = A\sqrt{k_0 m_0}. \tag{3}$$

The overall boundary condition at $x = 0$ therefore becomes

$$-Ak_0 y^I_x(0;s) = -z_0 s y^I(0;s) + \psi(s). \tag{4}$$

Since medium I is non-dispersive, (4) can be also regarded as a passive radiating boundary condition [35–37] having constant damping equal to the domain impedance z_0.

2.2.2. Modeling the metamaterial medium II

Here we model the target metamaterial that we want to obtain using feedback control, i.e. the desired closed loop system. It will have dynamic constitutive parameters, which for a unit cell are the mass $M_0\widetilde{M}(s)$ and stiffness $K_0\widetilde{K}(s)$. Following a similar approach to that used for medium I, the governing equations for medium II can be written as

$$f(x;s) = Ak_0\widetilde{K}(s) y^{II}_x(x;s), \tag{5a}$$

$$f_x(x;s) = Am_0\widetilde{M}(s) s^2 y^{II}(x;s). \tag{5b}$$

where y^{II} indicates the particle displacement. The dynamic extensions of the nominal constitutive parameters, $\widetilde{K}(s)$ and $\widetilde{M}(s)$, can be regarded as the local transfer functions from the displacement gradient to force, and from acceleration to the force gradient, respectively. Combining (5a) with (5b), we obtain

$$y^{II}_{xx}(x;s) = \frac{\alpha^2(s)}{c^2} y^{II}(x;s), \tag{6}$$

where

$$\alpha(s) = s\sqrt{\frac{\widetilde{M}(s)}{\widetilde{K}(s)}} \tag{7}$$

may be regarded as the dispersion relation. We now consider the end conditions of medium II. Continuity of displacement and force between the media at $x = x_0$ requires

$$y^I(x_0;s) = y^{II}(x_0;s), \tag{8a}$$

$$Ak_0 y^I_x(x_0;s) = Ak_0\widetilde{K}(s) y^{II}_x(x_0;s). \tag{8b}$$

Similarly to the boundary condition used at $x = 0$, at $x = L$ we employ an impedance matching boundary control to prevent reflections. Since the medium is now governed by an extended wave Eq. (6), we can no longer use the simple active damper as in (4). Following the results in [31,30,38] for boundary control of dispersive systems, we set the impedance matching controller at $x = L$ to a dynamic function, equal to the characteristic impedance of medium II, which is given by

$$z(s) = z_0\widetilde{Z}(s), \quad \widetilde{Z}(s) = \sqrt{\widetilde{M}(s)\widetilde{K}(s)} = \frac{\widetilde{K}(s)\alpha(s)}{s}. \tag{9}$$

where z_0 is the impedance of medium I, defined in (3), and $\alpha(s)$ is defined in (7). The boundary condition at $x = L$ becomes

$$Ak_0\widetilde{K}(s) y^{II}_x(L;s) = z_0\widetilde{Z}(s) s y^I(L;s). \tag{10}$$

We note that since medium II is despersive, achieving (10) by means of conventional passive boundary conditions is usually impossible, as the impedance $z(s)$ is generally of fractional order, see Section 3.

2.2.3. Overall transfer function model

Since usually the velocity is the output of interest, in particular in the analogous acoustic system, we write the system TF model in the two media for the velocity variable $v = sy$. Considering Eqs. (2), (4), (68) we obtain the velocity response of

media I and II to the source $\psi(s)$ as $v^I(x;s) = G^I(x;s)\psi(s)$ and $v^{II}(x;s) = G^{II}(x;s)\psi(s)$, respectively. The corresponding transfer functions are given by

$$G^I(x;s) = \frac{1}{2z_0}\left[e^{-\tau_x s} + R(s)e^{-\left(2\tau_{x_0}-\tau_x\right)s}\right] \tag{11a}$$

$$G^{II}(x;s) = \frac{1}{2z_0}T(s)e^{-\tau_{x_0}s}e^{-\left(\tau_x-\tau_{x_0}\right)\alpha(s)}, \tag{11b}$$

where $\tau_x = \frac{x}{c}$ and $\tau_{x_0} = \frac{x_0}{c}$ are time constants, and

$$T(s) = \frac{2}{\widetilde{Z}(s)+1}, \quad R(s) = T(s) - 1, \tag{12}$$

are the transmission and reflection coefficients of the system. The normalized impedance $\widetilde{Z}(s)$ and $\alpha(s)$ were respectively defined in (9) and (7). In closed loop the transfer functions $G^I(x;s)$ and $G^{II}(x;s)$ are infinite dimensional, explicitly indicating wave motion and capturing the entire transients and steady state response to external sources. Infinite dimensional and fractional order transfer functions of other systems with complex dynamics were reported also in [38,31,30]. The exponents in $G^I(x;s)$ and $G^{II}(x;s)$ represent the wave shape evolution during propagation along each medium, whereas the transmission and reflection coefficients $T(s)$ and $R(s)$ characterize the interface between media. Since we assumed in Section 2.2 that boundary impedance matching controllers are employed, there are no exponents in the denominators of $G^I(x;s)$ and $G^{II}(x;s)$. The combinations of time constants indicate the wave arrival times to the corresponding locations, as illustrated in Fig. 2 for the different wave paths. For example, $e^{-\tau_x s}$ of $G^I(x;s)$ represents a wave that is generated by the source ψ and travels from $x = 0$ to any x in medium I at τ_x seconds. Since in medium I there is no dispersion, the wave has constant velocity c. The exponent $e^{-\left(2\tau_{x_0}-\tau_x\right)s}$ represents the above wave when reflected from x_0 back to medium I (hence multiplied by $R(s)$). As for $G^{II}(x;s)$, the exponent $e^{-\tau_{x_0}s}e^{-\left(\tau_x-\tau_{x_0}\right)\alpha(s)}$ represents the source wave that is transmitted to medium II (after traveling for τ_{x_0} seconds in medium I). The dispersion of medium II is captured by $\alpha(s)$, the dispersion relation, and by the exponential term. Due to dispersion, only the wave head arrives at x after $\tau_x - \tau_{x_0}$ seconds, whereas the behavior of the rest of the wave is captured by $\alpha(s)$. $\alpha(s)$ is related to the wavenumber k of a commonly assumed steady state solution $e^{i(kx-\omega t)}$, where ω is the source signal frequency, via

$$k(i\omega) = \frac{\alpha(i\omega)}{ci} = \frac{\omega}{c}\sqrt{\frac{\widetilde{M}(i\omega)}{\widetilde{K}(i\omega)}}. \tag{13}$$

2.3. Closed loop metamaterial control design

In this section we design control algorithms for the controllers $C_j(s)$ in Fig. 1 in order to convert medium II into a target metamaterial system 6,7 using real time feedback loops. We carry out the derivation for general constitutive parameters $k(s)$ and $m(s)$. Controllers for specific parameters are designed in Section 3.2. A complete analysis of closed loop stability is given in Appendix A. Since the actuators are attached directly to the beam (gold squares in Fig. 1) we denote our control strategy by direct external control. In the absence of these control loops, medium II is characterized by the nominal constitutive parameters k_0 and m_0, as the other section of the beam. The previous consideration assumes that the local stiffening produced by surface-bonded actuators can be neglected. Several flexible actuators are available on the market that would satisfy this assumption. Otherwise, the local stiffening effect could also be easily introduced in the model. Since the actual actuation and measurement is spatially discrete, we design the control algorithms for a single unit cell, achieving the constitutive

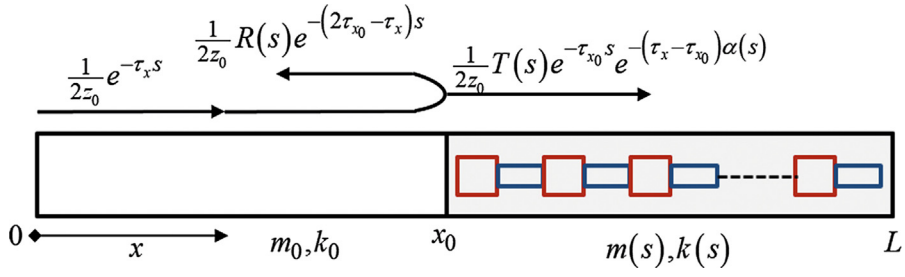

Fig. 2. Schematics indicating of incident, reflected, and transmitted waves in accordance with the transfer function model (11). Each wave is labeled by an arrow indicating its propagation direction and the corresponding propagation exponent. The arrival times are: τ_x and $2\tau_x - \tau_{x_0}$ for medium I respectively before and after reflection from x_0, and τ_x for medium II after transmission from x_0.

parameters $K(s)$ and $M(s)$, for which $k(s) = K(s)\mathrm{d}x$ and $m(s) = M(s)/\mathrm{d}x$ are the continuous limit. In the forthcoming derivations, we denote the j_{th} unit cell displacement by y_j^{II}. At each unit cell we employ a single actuator that is attached directly to the structure (each golden square in Fig. 1), and is designed to control simultaneously the stiffness and mass parameters. The goal is to convert, in the continuum limit, the nominal system $\{k_0, m_0\}$ to the target system $\{k(s), m(s)\}$, by a proper design of the controllers. Denoting the external control input by h_j, the governing equations for the j_{th} unit cell, which are the nominal (uncontrolled) form of Eqs. (5), become

$$f_{j+1} = AK_0\left(y_{j+1}^{II} - y_j^{II}\right) \tag{14a}$$

$$f_{j+1} - f_j = AM_0 s^2 y_j^{II} - h_j. \tag{14b}$$

We model h_j as an external input which affects the system through the mass Eq. (14b). A proper design of h can generate a desired expression for the dispersion $\alpha(s)$. We defining the collocated control law

$$h_j = -C_j(s)z_j = -C(s)v_j^{II}, \quad j = 2, \ldots, N-1 \tag{15}$$

where v_j^{II} is a velocity measurement. The controller

$$C(s) = AM_0 s\left[\frac{\widetilde{M}(s)}{\widetilde{K}(s)} - 1\right] = AM_0\frac{\alpha^2(s) - s^2}{s} \tag{16}$$

converts (14) into

$$AK_0\widetilde{K}(s)\left(y_{j+1}^{II} - 2y_j^{II} + y_{j-1}^{II}\right) = AM_0\widetilde{M}(s)s^2 y_j^{II}, \tag{17}$$

whose continuum limit coincides with (6). The choice of $\widetilde{M}(s)$ and $\widetilde{K}(s)$ must provide a causal $C(s)$. It is interesting to note that the controller in (16) might have zeros at frequencies ω_z, provided $\alpha^2(i\omega_z) = \omega_z^2$ has a solution. The control signal at these frequencies will then converge to zero at steady state. At the transition/end points, however, there is an individual influence of the effective stiffness, as stems from the continuity conditions at $x = x_0$, (8), and in the boundary conditions at $x = L$, (10). At the end unit cells $j = 1$ ($x = x_0$) and $j = N$ ($x = L$), the open loop system

$$AK_0\left(y_2^{II} - y_1^{II}\right) - AK_0\left(y_1^{II} - y_{N_1}^{I}\right) = AM_0 s^2 y_1^{II} - h_1, \tag{18a}$$

$$-AK_0\left(y_N^{II} - y_{N-1}^{II}\right) = AM_0 s^2 y_N^{II} - h_N, \tag{18b}$$

where $y_{N_1}^{I}$ is the displacement of the last point of medium I, needs to be converted to the target closed loop system

$$AK_0\widetilde{K}(s)\left(y_2^{II} - y_1^{II}\right) - AK_0\left(y_1^{II} - y_{N_1}^{I}\right) = AM_0\widetilde{M}(s)s^2 y_1^{II}, \tag{19a}$$

$$-AK_0\widetilde{K}(s)\left(y_N^{II} - y_{N-1}^{II}\right) = AM_0\widetilde{M}(s)s^2 y_N^{II}, \tag{19b}$$

using an appropriate choice of the control inputs h_1 and h_N. Controlling $\alpha(s)$ through $m(s)$ at the transition point then becomes insufficient (but still can be done at $x = L$ though in the absence of external inputs there). Therefore, at the end unit cells we define mixed control laws of the form

$$h_1 = -C_1(s)z_1 = -C_m(s)v_1^{II} - C_k(s)f_2, \tag{20a}$$

$$h_N = -C_N(s)z_N = -C_m(s)v_N^{II} + C_k(s)f_N, \tag{20b}$$

where $v_j^{II} = sy_1^{II}$. The measurements of the reaction forces f_2 and f_N are equivalent to $AK_0\left(y_2^{II} - y_1^{II}\right)$ and $AK_0\left(y_{N-1}^{II} - y_N^{II}\right)$, respectively, evolving into spatial derivatives at the continuous limit. The corresponding end point controllers are then given by

$$C_m(s) = AM_0 s\left(\widetilde{M}(s) - 1\right), \quad C_k(s) = 1 - \widetilde{K}(s). \tag{21}$$

The forces, or equivalently, the displacement gradients feedback in (20) represent the manipulation needed to compensate for the actuators h_1 and h_N not having an access to the stiffness Eq. (14a). Relations (17) and (19) therefore represent a beam of mass density m_0 and stiffness k_0, whose right section $x_0 \leqslant x \leqslant L$ is controlled in closed loop by periodically spaced actuators and as a result has the dynamic effective mass density $m_0\widetilde{M}(s)$ and stiffness $k_0\widetilde{K}(s)$. Denoting the position of the actual discrete actuator h_j by x_j, the resulting transfer functions from ψ to h_j then become

$$\frac{h_j(s)}{\psi(s)} = -\frac{1}{2z_0}T(s)e^{-\tau_{x_0}s}e^{-\left(\tau_{x_j}-\tau_{x_0}\right)\alpha(s)}\begin{cases} C_m(s) + \frac{1}{c}\alpha(s)C_k(s), & j = 1, \\ C(s), & j = 2, \ldots, N-1 \\ C_m(s) - \frac{1}{c}\alpha(s)C_k(s), & j = N. \end{cases} \tag{22}$$

In Appendix A we prove that the TFs in (22) are stable. The advantage of the direct external control approach of Section 2.3, which is suitable for the direct actuation setup proposed in this work is in the versatility it provides in the achievable constitutive parameters. Within the limits of available actuation effort, any desired expressions of $\widetilde{K}(s)$ and $\widetilde{M}(s)$ can be obtained, provided that the controllers are causal and the loop is stable. Since there are no built-in structural inclusions, there are no predefined expressions that the target parameters are obliged to follow. There is also a fabrication advantage, as the open loop system is a conventional continuous structure defined by $\{k_0, m_0\}$, with actuators spread along it. The drawback of this approach is the higher control effort that might be required to compensate for the lack of passive resonators.

3. Application to selected metamaterial configurations

3.1. The unit cell

In this section we analyze the wave propagation in the structure in Fig. 1 for effective constitutive parameters $k(s)$ and $m(s)$ obtained by the feedback loops therein. For the base structure we consider an aluminium rod of mass density $m_0 = 2700$ [kg], Young modulus $k_0 = 70 \cdot 10^9$ [N/m^2] and cross-section $A = 0.006 \cdot 0.02$ [m^2] (where A becomes relevant in Section 2.3 only), leading to $c \approx 5092$ [m/s]. $k(s) = k_0\widetilde{K}(s)$ and $m(s) = m_0\widetilde{M}(s)$ are the continuum limit of the unit cell parameters $K(s) = K_0\widetilde{K}(s)$ and $M(s) = M_0\widetilde{M}(s)$. Using spring-mass representation, the effective unit cell mass $M(s)$ is obtained by connecting M_0 to a spring K_m and a damper B_m, whose other end is fixed. The effective unit cell stiffness (spring) $K(s)$ is obtained when connecting K_0 to a spring K_h and a damper B_h, whose other end is connected to the successive unit cell. The relative displacement of K_h induces, through two lever arms, the displacement of a mass $\widehat{M}_h$, which is proportional to the double tangent of the lever arm angle θ with the x axis. We define $M_h \approx 2\widehat{M}_h \tan\theta$. Such an arrangement of $K(s)$ and $M(s)$ has analogies in other disciplines. The first example is the electro-magnetic metamaterial in the pioneering work [4] on left handed materials, where the effective permittivity and permeability respectively stand for the effective mass and stiffness of the mechanical unit cell in Fig. 3, and have the same expressions as in (24), derived below. Another example [12] is an electrical transmission line with a unit cell comprised of capacitors $\frac{1}{K_h}, \frac{1}{K_m}$ and inductance M_h related as in Fig. 3, that was suggested as a composite right/left handed electronic material. There is also an example in acoustics [17,14,13], where a tube with elastic membranes K_m and cavities (Helmholtz resonators) K_h, M_h was considered as an acoustic metamaterial with a similar type of unit cell. We now derive explicit expressions for $K(s)$ and $M(s)$. Applying a force balance to both masses M_0 and M_h, and at the point connecting the springs K_0 and K_h, we obtain the associated unit cell impedance relations $z_h(s) = M_h s + B_h + \frac{K_h}{s}$ and $z_m(s) = M_0 s + B_m + \frac{K_m}{s}$. Defining the corresponding densities $k_m = K_m/\mathrm{d}x, b_m = B_m/\mathrm{d}x$, $k_h = K_h\mathrm{d}x, m_h = M_h\mathrm{d}x$ and $b_h = B_h\mathrm{d}x$, and the consequent normalized parameters

$$\omega_m^2 = \frac{k_m}{m_0}, \quad \omega_h^2 = \frac{k_h}{m_h}, \quad \omega_b^2 = \omega_h^2(1+b), \quad b = \frac{k_0}{k_h}, \quad \zeta_m = \frac{b_m}{2\omega_m m_0}, \quad \zeta_h = \frac{b_h}{2\omega_h m_h}, \quad \zeta_b = \frac{b_h}{2\omega_b m_h}, \tag{23}$$

the resulting normalized effective stiffness and mass take the form

$$\widetilde{K}(s) = \frac{sz_h(s)}{K_0 + sz_h(s)} = \frac{s^2 + 2\zeta_h\omega_h s + \omega_h^2}{s^2 + 2\zeta_b\omega_b s + \omega_b^2}, \tag{24a}$$

$$\widetilde{M}(s) = \frac{z_m(s)}{M_0 s} = \frac{s^2 + 2\zeta_m\omega_m s + \omega_m^2}{s^2}. \tag{24b}$$

As shown in the discussion below, the form of $\widetilde{K}(s)$ and $\widetilde{M}(s)$ in (24) give rise to different interesting working regimes. However, a particular special regime is obtained when $\omega_m = \omega_b$ (leading also to $\zeta_m = \zeta_b$) so this is our assumption in the

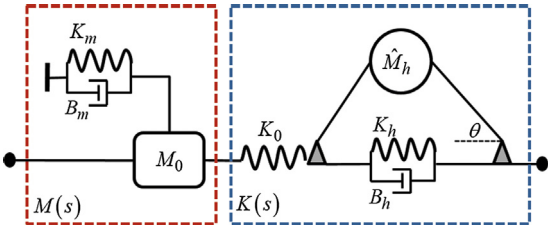

Fig. 3. Spring-mass representation of a possible unit cell of the mechanical metamaterial in Fig. 1. The effective mass $M(s) = M_0\widetilde{M}(s)$ (red box) comprises the original mass M_0 attached to a fixed wall through a spring K_m and a damper B_m. The effective stiffness $K(s) = K_0\widetilde{K}(s)$ (blue box) comprises the original spring K_0, connected in series to another spring K_h and damper B_h, and induces a corresponding motion of a mass $M_h \approx 2\widehat{M}_h \tan\theta$. The explicit expressions for $M(s)$ and $K(s)$ are given in (24). (For interpretation of the references to colour in this figure legend, the reader is referred to the web version of this article.)

following. For brevity, we also assume that $B_m = B_h$, leading to $\zeta_h = \zeta_m \frac{\omega_m}{\omega_h}$. The propagation exponent in (7) and the impedance in (9) then take the form

$$\alpha(s) = \frac{s^2 + 2\zeta_m\omega_m s + \omega_m^2}{\sqrt{s^2 + 2\zeta_h\omega_h s + \omega_h^2}}, \quad \widetilde{Z}(s) = \frac{\sqrt{s^2 + 2\zeta_h\omega_h s + \omega_h^2}}{s}. \tag{25}$$

Both $\alpha(s)$ and $\widetilde{Z}(s)$ in (25) are of fractional order, implying that the transfer functions $G^I(x;s)$ and $G^{II}(x;s)$ in (11) are of fractional order. From time domain considerations, $\alpha(s)$ determines the entire time response through the inverse Laplace transform of the propagation exponent $e^{-(\tau_x-\tau_{x_0})\alpha(s)}$ in (11b), which is expected to give rise to special functions (see [31,30] for analysis of fractional order transfer functions of similar kind involving Bessel functions). From frequency domain considerations (steady state response), the fractional order of $\alpha(s)$ indicates the dispersion in medium *II* due to the dynamic $\widetilde{M}(s)$ and $\widetilde{K}(s)$, as implied by the wavenumber relation (13). The effect of the specific constitutive parameters in (24) on the wavenumber k is illustrated in Fig. 4-**(a)** for the parameters $f_h = \omega_h/2\pi = 1.323$ [kHz], $b = 3$ and $\zeta_m = 0.01$, leading to $f_m = \omega_m/2\pi = 2.646$ [kHz] and $\zeta_h = 0.02$. It depicts the Bode plot of normalized effective stiffness $\widetilde{K}(s)$ (blue) and mass $\widetilde{M}(s)$ (red), the dispersion function $\alpha(s)$ (black), wavenumber $k(i\omega)c$ (grey) and the nominal wavenumber k_{nom} (green) for comparison. While $\widetilde{M}, \widetilde{K}$ and α are independent of the base beam material, k and k_{nom} do depend on it through c.

In the forthcoming discussion ζ_m and ζ_h are ignored, however we keep in mind that some damping always exists, maintaining the transfer functions in (11) stable, so that the response indeed reaches steady state. A rigorous stability analysis is given in Appendix A. We focus the following discussion on the existence of four different regions in Fig. 4-**(a)** that correspond to four different regimes of operation of the active metamaterial.

Regime 1: $0 < \omega < \omega_h$. The phase of the effective mass $\widetilde{M}(i\omega)$ is 180°, whereas the phase of $\widetilde{K}(i\omega)$ is 0°, indicating that $\widetilde{M}(i\omega)$ is negative and $\widetilde{K}(i\omega)$ is positive (zero at $\omega = \omega_h$). Medium *II* is thus a negative-mass positive-stiffness metamaterial. The phase of $\alpha(i\omega)$ is 0°, i.e. it is positive (equivalently, $k(i\omega)$ is pure imaginary due to 90° phase). According to the transfer function in (11b), no wave propagation is thus possible in medium *II* at this frequency range. The wave decay rate is determined by the amplitude of $\alpha(i\omega)$, which increases as ω approaches ω_h ($\widetilde{K}(i\omega)$ approaches zero). This regime is useful for wave isolation applications.

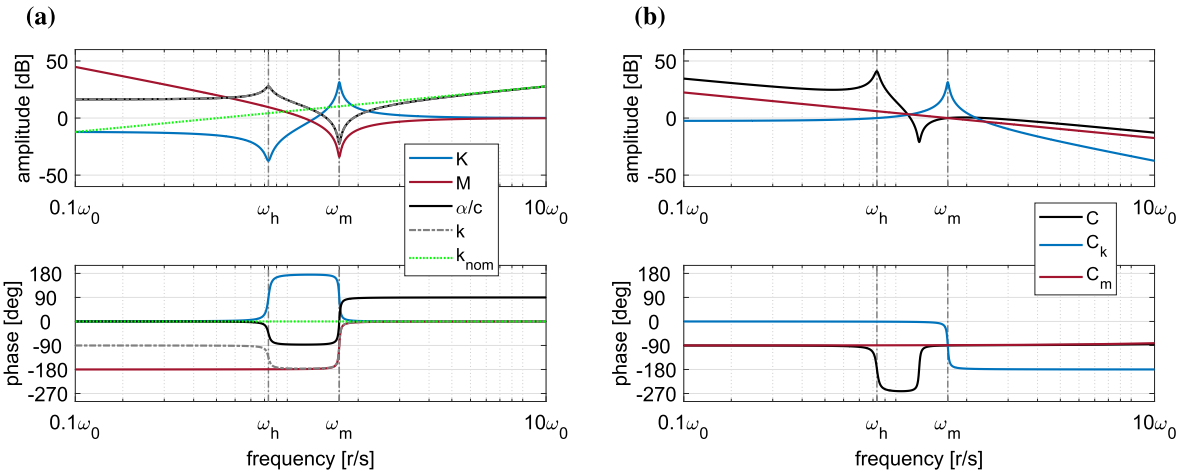

Fig. 4. (a). Illustration of the different working regimes of the mechanical metamaterial in Section 3. Plots illustrate the frequency response diagrams of the normalized effective stiffness $\widetilde{K}(s)$ (blue) and mass $\widetilde{M}(s)$ (red) in (24), the resulting dispersion function $\alpha(s)$ (black) in (25) and the wavenumber k (grey) in (13) for $f_h = 1.323$ [kHz], $\zeta_m = 0.01, f_m = 2.646$ [kHz] and $\zeta_h = 0.02$. The nominal wavenumber k_{nom} (green) of medium *II* is given for comparison. We distinguish between the following four regimes. **Regime 1:** $0 < \omega < \omega_h$. $\widetilde{M}(i\omega) < 0, \widetilde{K}(i\omega) > 0, \alpha(i\omega) > 0$ and $k(i\omega) \propto i$. This is the negative mass, positive stiffness (zero at ω_h) regime. All waves decay, hence wave propagation is blocked. Highest decay rate is at $\omega = \omega_h$ ($\widetilde{K}(i\omega_h) \to 0, \alpha(i\omega_h) \to \infty$). **Regime 2:** $\omega_h < \omega < \omega_m$. $\widetilde{M}(i\omega) < 0, \widetilde{K}(i\omega) < 0, \alpha(i\omega) \propto i$ and $k(i\omega) < 0$. This is the double-negative regime. Waves propagate with a negative phase velocity. **Regime 3:** $\omega = \omega_m$. $\widetilde{M}(i\omega) \to 0$ and $\widetilde{K}(i\omega) \to \infty$. This transition point is denoted by the "double-zero" regime, for a zero mass and a zero inverse stiffness. Since $\alpha(i\omega_m) \to 0$, the transfer function (11b) becomes independent of x, as if medium *II* was a rigid body. **Regime 4:** $\omega_m < \omega < \infty$. $\widetilde{M}(i\omega) > 0, \widetilde{K}(i\omega) > 0, \alpha(i\omega) \propto i$ and $k(i\omega) > 0$. This is a double positive regime, indicating wave propagation with positive phase velocity. In all regimes k_{nom} is positive and increases with ω, eventually aligning with k (in regime 3). **(b)**. Frequency response diagram of the controllers in (26), which generate the target constitutive parameters in (24): $C(s)/M_0$ (black), $C_k(s)$ (blue) and $C_m(s)/M_0$ (red). $C(s)$ has a pole at $\sim \omega_h$, leading to highest control signals h_j in (22), $j = 2, \ldots, N-1$, at this frequency (regime 1). At ω_z, the zero of $C(s)$ (regime 2), $h_j, j = 2, \ldots, N-1$, decay to zero at steady state. Although $K(i\omega)$ has a pole at ω_m (regime 3), $C(s)$ does not, hence $h_j, j = 2, \ldots, N-1$, are not the highest there. Only the end controller $C_k(s)$ has a pole at ω_m, implying h_1 and h_N are the highest at ω_m. $C_m(s)$ has a pole only at the origin. (For interpretation of the references to colour in this figure legend, the reader is referred to the web version of this article.)

Regime 2: $\omega_h < \omega < \omega_m$. Both $\widetilde{K}(i\omega)$ and $\widetilde{M}(i\omega)$ are negative (phases 180° and −180°, respectively). The phase of $\alpha(i\omega)$ is −90°, and, equivalently, the phase of $k(i\omega)$ is −180°, yielding a negative wavenumber. The system therefore supports backward wave propagation in steady state with a negative phase velocity $v_{ph} = \omega/k(i\omega) < 0$. In this regime, medium *II* behaves as a negative-phase-velocity metamaterial.

Regime 3: $\omega = \omega_m$. At this frequency we have a sharp transition from the doubly-negative to the doubly-positive region, with $\widetilde{M}(i\omega) = 0$ and $\widetilde{K}(i\omega) \to \infty$. This special regime is referred in the literature as a double-zero metamaterial (meaning zero mass and zero inverse stiffness) [21]. At this frequency, $\alpha(i\omega_m) \to 0$. The implication is that the transfer function (11b) becomes independent of x, and medium *II* thus behaves as a rigid body (i.e. infinite phase velocity).

Regime 4: $\omega_m < \omega < \infty$. Here both $\widetilde{M}(i\omega)$ and $\widetilde{K}(i\omega)$ are positive (phase 0°), and so is $k(i\omega)$. On the contrary, $\alpha(i\omega)$ is imaginary therefore yielding a conventional positive-mass positive-stiffness material. Note that dispersion still exists where the positive phase velocity decreases with frequency (as the amplitude of $k(i\omega)$ increases).

We now discuss the impedance $z(s)$ and the transmission coefficient $T(s)$ in (25). At $0 < \omega < \omega_h$ (regime 1), $|\widetilde{Z}(i\omega)|$ decreases from infinity to zero, resulting in $|T(i\omega)|$ increasing from zero to 2. Wave propagation is still blocked at $\omega = \omega_h$ due to the propagation exponent $e^{-(\tau_x - \tau_{x_0})\alpha(i\omega)}$, which then approaches zero. At $\omega_h < \omega < \infty$ (regimes 1, 2 and 3), $|\widetilde{Z}(i\omega)|$ increases and $|T(i\omega)|$ decreases monotonically to 1. It is interesting to note that at $\omega = \omega_m$ we obtain $\widetilde{Z}(i\omega) = \sqrt{b/(1+b)}$.

3.2. The corresponding control design

In this section we obtain the explicit form of the controllers derived in Section 2.3 for the particular unit cell design presented in Section 3 and illustrated in Fig. 3. The resulting closed loop is proved in Appendix A to be stable. The main field controller in (16) and the end point controllers in (20) become

$$C(s) = AM_0 \frac{2\zeta_m\omega_m s^3 + (2\omega_m^2 + 4\zeta_m^2\omega_m^2 - \omega_h^2)s^2 + 4\zeta_m\omega_m^3 + \omega_m^4}{s(s^2 + 2\zeta_h\omega_h s + \omega_h^2)}, \tag{26a}$$

$$C_m(s) = AM_0 \frac{2\zeta_m\omega_m s + \omega_m^2}{s}, \tag{26b}$$

$$C_k(s) = \frac{2(\zeta_m\omega_m - \zeta_h\omega_h)s + \omega_m^2 - \omega_h^2}{s^2 + 2\zeta_m\omega_m s + \omega_m^2}. \tag{26c}$$

All the controllers in (26) are causal. The frequency response diagram of the controllers in (26) for $f_h = 1.323$ [kHz], $\zeta_m = 0.01$, $f_m = 2.646$ [kHz] and $\zeta_h = 0.02$, is illustrated in Fig. 4-**(b)**, with $C(s)/M_0$ (black), $C_k(s)$ (blue) and $C_m(s)/M_0$ (red). The main field controller $C(s)/M_0$ has a pole near ω_h, hence highest control signals $h_j, j = 2, \ldots, N-1$, in (22) are expected at this frequency, effectively to generate regime 1. Another pole is at $s = 0$. It also has a zero at ω_z, which tends to $(1+b)/\sqrt{1+2b}$ as damping becomes smaller and falls within the double-negative region (regime 2). This implies that we can turn medium *II* into a negative phase velocity metamaterial with no control effort in steady state (clearly, a transient effort is still required). Although $K(i\omega)$ has a pole at ω_m, $C(s)$ does not, hence $h_j, j = 2, \ldots, N-1$, are not the highest there (regime 3). Only the end controller $C_k(s)$ has a pole at ω_m, implying h_1 and h_N are the highest at ω_m. $C_m(s)$ has a pole only at the origin. All the three controllers in (26) introduce phase lag to the open loop system.

4. Numerical simulations of the active metamaterial

In this section we simulate the system in Fig. 1 when operated in closed loop according to the direct external control design in Section 2.3. The target closed loop constitutive parameters are given in (24) and the particular controllers are given in (26). The physical parameters of the nominal structure are given by $m_0 = 2700$ [kg], $k_0 = 70 \cdot 10^9$ [N/m^2] and $A = 0.006 \cdot 0.02$ [m^2], leading to $c \approx 5092$ [m/s]. The total length of the structure is $L = 1$ [m], where the controlled section, medium *II*, begins at $x_0 = 0.5$ [m]. The spacing of the cells in medium *II* is set to $\mathrm{d}x = 0.05$ [m], implying a total of $N = 11$ actuators. We denote this setup by the actual metamaterial. For this spacing to be a sub-wavelength periodic structure, the supported wavelength should be at least four times longer [10], i.e. $\lambda \geqslant 0.2$ [m], which implies a maximum wavenumber of $k \leqslant 10\pi[1/m] \approx 30$ [dB].

In the simulations of Fig. 5 we wish to demonstrate the main achievement of our control design that is the ability of the active metamaterial to obtain desired constitutive parameters only by an appropriate choice of the controllers. We choose four different sets of the parameters in (26) so that our system can operate at any of the four regimes described in Section 3 for a fixed frequency source. We consider a source ψ of frequency $f = 2$ [kHz] at $x = 0$, four different characteristic frequencies $f_h = \omega_h/2\pi$, respectively given by $f_h = \{2.2, 1.32, 1, 0.5\}$ [kHz], and the fixed values $b = 3$ and $\zeta_m = 0.01$. This implies $\zeta_h = 0.02$ and $f_m = 2f_h = \{4.4, 2.64, 2, 1\}$ [kHz], leading to four different working regimes, as discussed in Section 3: negative effective mass, as well as double negative, double zero, and double positive effective parameters (i.e. mass and stiffness). The system consists of the aluminium rod considered in Section 3 with the nominal parameters $m_0 = 2700$ [kg] and

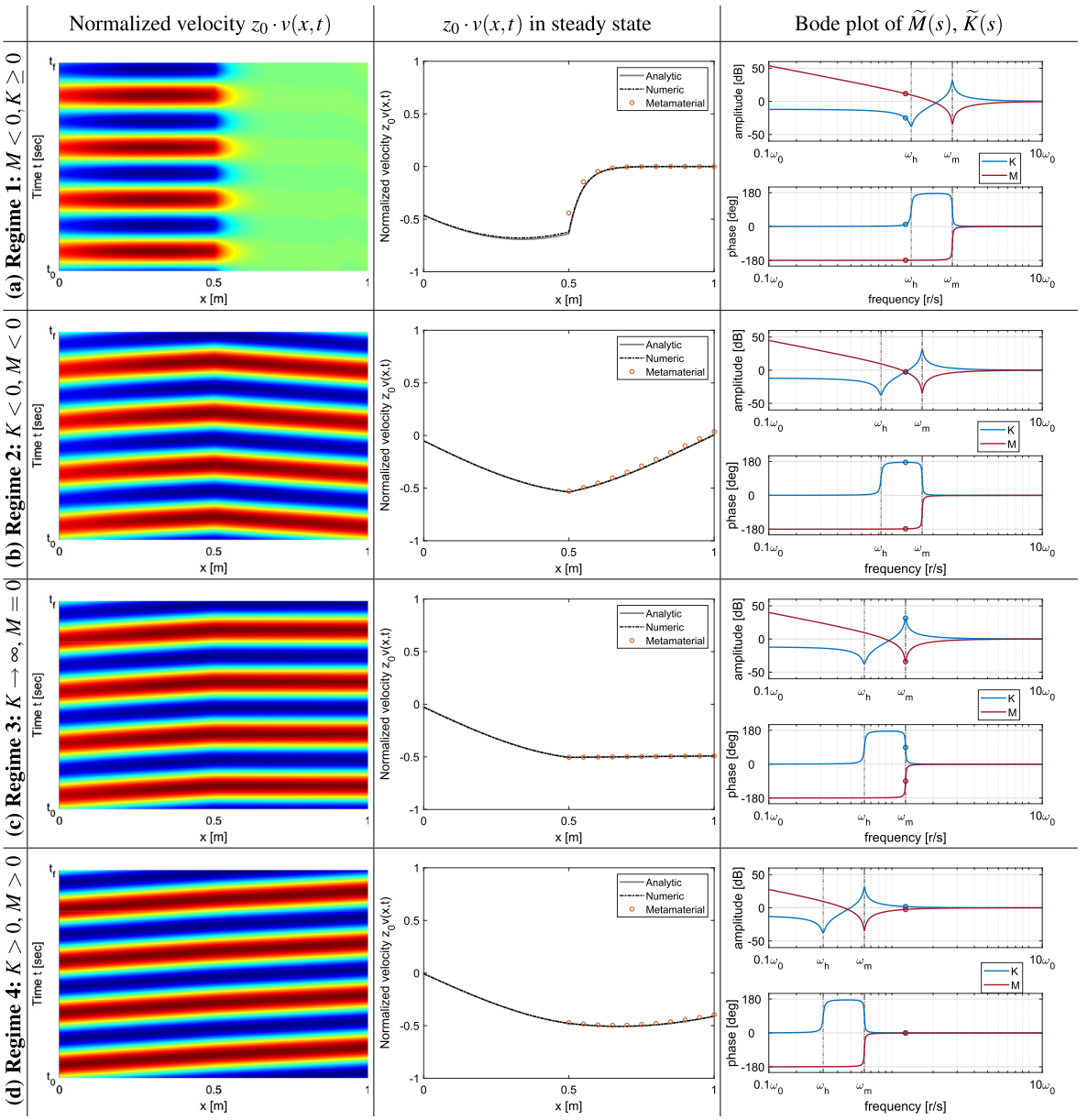

Fig. 5. Simulation of the feedback-based metamaterial in Fig. 1, comprising an Aluminium rod with 11 actuators evenly spanned between $x_0 = 0.5$ [m] and $L = 1$ [m]. The system is generated by the control algorithm in (15), (20), and (26). Four different controller parameters $f_h = \{2.2, 1.32, 1, 0.5\}$ [kHz] and fixed $b = 3, \zeta_m = 0.01$ are considered, leading to $f_m = \{4.4, 2.64, 2, 1\}$ [kHz]. This implies four different working regimes for a source frequency $f = 2$ [kHz] (acting at $x = 0$), which is marked in the right column on top of the Bode plots of the resulting $\widetilde{K}(s) = k(s)/k_0$ (blue) and $\widetilde{M}(s) = m(s)/m_0$ (red). The middle column depicts steady state velocity response, comparing analytic TF (11) (solid), numeric with spacing $dx = 0.001$ [m] (dashed-dotted) and actual metamaterial with spacing $dx = 0.05$ [m] (circles). Left column depicts the response in a 2*D* space–time plot. **(a) Regime 1:** $m < 0, k > 0$. Wave propagation is blocked, decaying significantly at about $x_0 + 0.1$ [m]. **(b) Regime 2:** $m < 0, k < 0$. Double-negative regime. Waves propagate with negative phase velocity. The slope of the equal amplitude lines in the 2*D* plot turns negative at $x_0 \leqslant x \leqslant L$. **(c) Regime 3:** $m \to 0, k \to \infty$. Double-zero regime. The metamaterial vibrates as a rigid body. 2*D* plot slope turns zero at $x_0 \leqslant x \leqslant L$. **(d) Regime 4:** $m > 0, k > 0$, as in a conventional material. 2*D* plot slope changes but remains positive at $x_0 \leqslant x \leqslant L$. (For interpretation of the references to colour in this figure legend, the reader is referred to the web version of this article.)

$k_0 = 70 \cdot 10^9$ [N/m^2]. The corresponding unit cell nominal parameters then become $M_0 = 135$ [kg · m] and $K_0 = 1.4 \cdot 10^{12}$ [N/m^3]. The response of the system is simulated for $t_f = 0.02$ [s]. The results of the simulations are summarized in Fig. 5. Column **(a)** depicts the velocity response of the entire beam ($0 \leqslant x \leqslant L$) in a two-dimensional plot as a function of space and time, where the time axis is shown only for its last 20%. Column **(b)** depicts a snapshot of the entire beam velocity response at steady state. The response of the actual 0.05 [m] spacing metamaterial (orange circles) is compared to the numeric response of the continuum limit (a 0.001 [m] spacing, black dashed-dotted lines), and to the exact analytic solution

given by the transfer functions in (11) (grey solid lines). Column **(c)** depicts the frequency response of the closed loop effective constitutive parameters in (24) (blue – $\widetilde{K}(i\omega)$, red – $\widetilde{M}(i\omega)$). The working frequency $f = 2$ [kHz] is marked on both $\widetilde{K}$ and $\widetilde{M}$ curves, indicating the relevant region out of the four regions listed in Section 3. In all the four cases the waves propagate in the dispersion-less medium I with phase velocity $c = 5092$ [m/s] and a corresponding wavelength $\lambda = 2.55$ [m]. They are partially reflected at $x = x_0$ according to (12) and are absorbed at $x = 0$ due to the embedded impedance matching boundary controller defined in (4). The waves at $x = L$ are fully absorbed by the boundary control defined in (10).

The control signals $h_j(t)$ are depicted in Fig. 6. They are calculated according to the laws (15) and (20), and given in analytical form by (22). The force feedback of the end signals h_1 and h_N in (20) is calculated as a spatial difference $AK_0(y^{II}_2 - y^{II}_1)$ and $AK_0(y^{II}_{N-1} - y^{II}_N)$, respectively. Regimes $1, 2, 3, 4$ are respectively depicted in plots **(a)**, **(b)**, **(c)** and **(d)**. The dashed-dotted grey lines mark the unit amplitude threshold, within which the control signals can be generated by the same actuators that produce the source ψ. The individual conclusions for the four regimes, respectively plotted in the four lines **(a)**, **(b)**, **(c)** and **(d)** of Fig. 5 and of Fig. 6, are ordered below.

(a) – regime 1. $f_h = 2.2$ [kHz] and $f_m = 4.4$ [kHz]. Fig. 5-**(a)**: the controller creates $K(i\omega) > 0$ and $M(i\omega) < 0$, i.e. positive spring – negative mass regime. As was discussed in Section 3, in this regime there is no wave propagation in medium II, where waves that are transmitted to $x_0 \leqslant x \leqslant L$ have a real positive $\alpha(i\omega)$ and decay according to the transfer function model (11). At $f = f_h$ we have $K(i\omega) = 0$ and thus $\alpha(i\omega)$ that approaches zero. Therefore, the closer f is to f_h, the faster is the decay. In our case a significant decay is obtained at about 10 $[cm]$ after x_0, as stems from the corresponding $2D$ plot. Fig. 6-**(a)**: since in this regime the velocity response is decaying, the control signals amplitudes decrease as actuators position approaches $x = L$. The amplitudes that are greater than 1 are those of h_1 (blue) and h_2 (orange). The value of h_j will

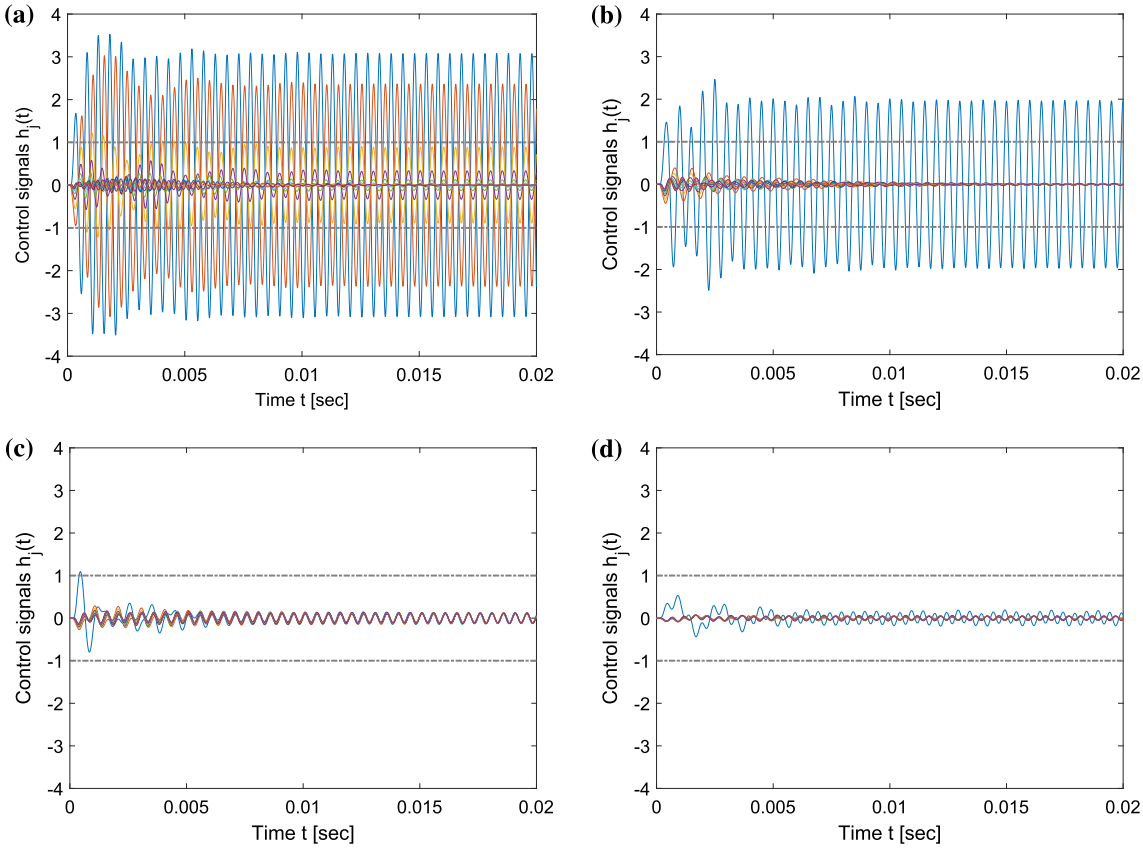

Fig. 6. Control signals $h_j(t), j = 1, \ldots, N$, of the simulations in Fig. 5, calculated according to the laws (15) and (20), and analytically given by (22). Regimes 1, 2, 3, 4 are respectively depicted in plots **(a)**, **(b)**, **(c)** and **(d)**. Signals with amplitudes 1 or smaller (within dashed-dotted grey lines) can be generated by the same actuators that produce the source ψ. **(a) – regime 1**, negative mass: Due to the decaying velocity response, the control signals amplitudes decrease as actuators position approaches $x = L$. The amplitudes that are greater than 1 are those of h_1 (blue) and h_2 (orange). **(b) – regime 2**, double negative: The system is simulated at f_z, the frequency at which the $j = 2, \ldots, N-1$ cells controller (16) has a zero. The respective signals h_j decay to zero at steady state. h_1 (blue) oscillates within ± 2. **(c) – regime 3**, double zero: All h_j oscillate below ± 1, with highest transient amplitude for h_1 (blue). **(d) – regime 4**, double positive: As k approaches k_{nom} (Fig. 4), all h_j oscillate considerably below ± 1. (For interpretation of the references to colour in this figure legend, the reader is referred to the web version of this article.)

increase when f approaches f_h due to the controller's pole at f_h, and will ultimately be determined by the damping ratio ζ_h.

(b) – regime 2. $f_h = 1.32$ [kHz] and $f_m = 2.64$ [kHz]. Fig. 5-**(b)**: the controller creates both $K(i\omega) < 0$ and $M(i\omega) < 0$, leading to the double negative regime. According to Section 3, in this regime the steady state propagation in medium *II* has a negative phase velocity, which is expressed through the negative slope of the equal amplitude lines at the corresponding 2*D* plot. Fig. 6-**(b)**: for the given f_h, we obtain $f = f_z$, where f_z is the zero of the $j = 2, \ldots, N-1$ cells controller (16), and the effective and the nominal wavenumbers k and k_{nom} intersect. The respective signals h_j therefore decay to zero, implying that no control effort is required at steady state to obtain this particular double negative metamaterial. The end control signal h_1 (blue) oscillates within ± 2.

(c) – regime 3. Fig. 5-**(c)**: the controller creates $K(i\omega) \to \infty$ and $M(i\omega) \to 0$, designated by the double zero regime. In this regime $\alpha(i\omega) = 0$ and (11b) becomes independent of x. According to the analysis in Section 3, every section of the metamaterial then vibrates in phase (as a rigid body) at a constant velocity for all $x_0 \leqslant x \leqslant L$. Therefore, the slope of the equal amplitude lines at the corresponding 2*D* plot turns zero at medium *II*. This result is consistent with the static-like behavior observed in double-zero metamaterials where the phase velocity diverges and the group velocity is progressively reduced to zero [39]. Fig. 6-**(c)**: all the control signals h_j remain within ± 1, where the highest amplitudes are obtained for the end signal h_1 (blue).

(d) – regime 4. Fig. 5-**(d)**: the controller creates both $K(i\omega) > 0$ and $M(i\omega) > 0$, i.e. a doubly positive regime. Here the steady state wave propagates forward with a positive phase velocity, which is expressed through the positive slope of the equal amplitude lines of the corresponding 2*D* plot. Fig. 6-**(d)**: as indicated by Fig. 4, in this regime as the working frequency increases, k approaches k_{nom}. The required control effort thus decreases accordingly, yielding the control signals h_j to oscillate considerably below ± 1.

5. Conclusion

We considered the problem of converting a mechanical structure, which in its nominal state is governed by the second order wave equation, into an active (tunable and reconfigurable) metamaterial using feedback control. The representative example for the nominal system is a beam in axial vibration. We designed a control algorithm that was capable to achieve different unconventional constitutive parameters (i.e. different effective dynamic stiffness and mass) for the same operating frequency. Such properties can be activated, deactivated, or tuned in real-time given that the design does not require any passive periodic feature embedded in the host structure, unlike traditional metamaterial designs. We showed by using numerical simulations that the control design was capable of obtaining a variety of conditions including negative effective mass (useful for wave propagation suppression), zero stiffness and negative mass (useful for total wave blocking), double negative parameters (i.e. negative phase velocity that results in backward wave propagation), and double zero properties for total impedance matching. We considered an external actuation approach, which consists in bonding actuators in periodic patterns to an initially homogeneous beam. This design enables large flexibility in terms of achievable effective constitutive parameters, that are only limited by the actuators gain capabilities. We derived the continuum model of the overall system in the form of fractional order transfer functions, which explicitly exhibited the special wave characteristics of the system, including the dispersion function, time delays, transmission and reflection coefficients. We used the transfer function model to explore the transmission and reflection properties between the controlled part of the beam (the metamaterial) and its uncontrolled part (a conventional medium). We proved that the closed loop system is stable and verified the control algorithm performance using numerical simulations.

Acknowledgements

This work was supported by the National Science Foundation through the EAGER Grant, award number 1745547.

Appendix A. Closed loop stability analysis

In this section we prove the stability of the closed loop system generated by the feedback control algorithm of Section 2.3. The control setup consists of a continuous beam, N concentrated actuators $h_j, j = 1, \ldots, N$, and respective N measurements, as illustrated in Fig. 1. The controllers $C(s), C_m(s)$ and $C_k(s)$ correspond to the direct external control strategy, specified by (15), (16), (20) and (21). The closed loop transfer functions from a source ψ to the velocity response and to the control inputs were derived in (11) and (22), respectively. The complete transfer matrix between all possible signals in the closed loop, including unmodeled signals such as actuation uncertainties and measurement noise, is given by

$$\begin{bmatrix} \mathbf{v} \\ \mathbf{h} \end{bmatrix} = \begin{pmatrix} \mathbf{G_{yd}} & \mathbf{G_{yn}} \\ \mathbf{G_{hd}} & \mathbf{G_{hn}} \end{pmatrix} \begin{bmatrix} \mathbf{d} \\ \mathbf{n} \end{bmatrix}. \tag{A.1}$$

Here $\mathbf{v} = \left[v^I(x;s)\ v^{II}(x;s) \right]'$ is the outputs vector including the axial vibration velocity at any location x along the beam. $\mathbf{h} = \left[h_1(s)\ h_j(s)\ h_N(s) \right]', j = 2, \ldots, N-1$, is the controls vector. $\mathbf{d} = \left[\psi(s)\ d_j(s) \right]', j = 1, \ldots, N$, is a representative external inputs

signal that stands for the source ψ and possible actuation disturbances d_j. $\mathbf{n} = \left[n_1(s)\ n_j(s)\ n_N(s)\right]', j = 2, \ldots, N-1$, is the measurement noises vector. The sub-matrices in (A.1) are given by

$$\begin{aligned} \mathbf{G_{yd}} &= \begin{bmatrix} G^I(x;s) & G^I_d(x;s) \\ G^{II}(x;s) & G^{II}_d(x;s) \end{bmatrix}, \qquad \mathbf{G_{yn}} = -\begin{bmatrix} G^I_d(x;s) \\ G^{II}_d(x;s) \end{bmatrix}\mathbf{C}, \\ \mathbf{G_{hd}} &= -\mathbf{C}'\begin{bmatrix} G^{II}(x;s) & G^{II}_d(x;s) \end{bmatrix}, \qquad \mathbf{G_{hn}} = -\mathbf{C}'\mathbf{G}_n(x;s), 2 \end{aligned} \tag{A.2}$$

where $G^I(x;s)$ and $G^{II}(x;s)$ are defined in (11a) and (11b), and $G^I_d(x;s), G^{II}_d(x;s)$ and $\mathbf{G}_n(x;s)$ are respectively given by

$$\begin{bmatrix} G^I_d(x;s) \\ G^{II}_d(x;s) \end{bmatrix} = \frac{1}{2z_0}\begin{bmatrix} T(s)e^{-\left(\tau_{x_0}-\tau_x\right)s}e^{-\left(\tau_{x_j}-\tau_{x_0}\right)\alpha(s)} \\ \frac{1}{Z(s)}\left(e^{-\left|\tau_x-\tau_{x_j}\right|\alpha(s)} + R(s)e^{-\left|\tau_x+\tau_{x_j}-2\tau_{x_0}\right|\alpha(s)}\right) \end{bmatrix}, j = 1, \ldots, N \tag{A.3a}$$

$$\mathbf{G}_n(x;s) = T(s)\begin{bmatrix} e^{-\left(\tau_{x_1}-\tau_{x_0}\right)(\alpha(s)-s)} & e^{-\left(\tau_{x_j}-\tau_{x_0}\right)(\alpha(s)-s)} & e^{-\left(\tau_{x_N}-\tau_{x_0}\right)(\alpha(s)-s)} \end{bmatrix}', j = 2, \ldots, N-1. \tag{A.3b}$$

In this section, we show that the complete closed-loop system (A.1)–(A.3)) is stable invoking the internal stability criterion, which claims that the closed loop system is stable provided that TFs from all possible inputs to all possible outputs are stable. These, in turn, are captured by the transfer matrix in (A.1), which consists of finite summations or multiplications of

$$G_1(s) = e^{-\theta\alpha(s)}, \quad G_2(s) = e^{-\theta(\alpha(s)-s)}, \quad G_3(s) = \widetilde{Z}^{-1}(s), \quad G_4(s) = T(s), \tag{A.4}$$

where by (12), stability of $R(s)$ stems directly from that of $T(s)$. The argument θ represents the various combinations of the time constants in (A.3). The goal of this section is therefore proving stability of each of the systems listed in (A.4), as stated in the following proposition.

Proposition A.1. *All the components of the complete closed loop system (A.1), which are given by the fractional order TFs in (A.4), are stable.*

Proof. Since the underlying TFs are all irrational, their stability analysis cannot, in general, be limited to pole location only. It could be therefore carried out either in frequency domain via the H^∞ criterion or in time domain via the L^1 criterion, as was discussed in [40]. For the L^1 criterion the inverse Laplace transforms of the TFs are required, which is nontrivial to obtain for fractional order systems. This was the approach for systems similar to (A.4) in [31,30]. Here we invoke the H^∞ criterion, and prove that the systems in (A.4) are analytic and bounded in the open right half plane.

Stability proof of $G_1(s)$. The branch points, which are the zeros of the square roots in $\alpha(s)$, defined in (7), are located in the open left half plane, and approach the imaginary axis as the damping approaches zero. Hence, $G_1(s)$ is analytic in the open right half plane. To prove that $|G_1(s)|$ is bounded in the open right half plane, it is sufficient to show that $\alpha(s)$ is non-negative for all $s = \sigma + \omega i$, where $\sigma > 0$, implying that $|G_1(s)| \leqslant 1$. Suppressing the damping for brevity, we define the mappings $z_m = s^2 + \omega_m^2$ and $z_h = s^2 + \omega_h^2$. We then denote the angles of $\alpha(s), z_m, z_h$ and z by $\phi_\alpha, \phi_m, \phi_h$ and ϕ, respectively. Since the angle of $\sqrt{z_h}$ is given by $\frac{1}{2}\phi_h$, we obtain $\phi_\alpha = \phi_m - \frac{1}{2}\phi_h$. We need to prove that $\phi_\alpha < \frac{1}{2}\pi$. Now, we have $0 \leqslant \phi < \frac{1}{2}\pi$. Since we also have $\omega_h < \omega_m$ by the definition in Section 3, we obtain the relation $\phi_m \leqslant \phi_h \leqslant 2\phi < \pi$. This implies $\frac{1}{2}\phi_m \leqslant \frac{1}{2}\phi_h$ and $\frac{1}{2}\phi_m < \frac{1}{2}\pi$, and therefore $\phi_\alpha = \phi_m - \frac{1}{2}\phi_h \leqslant \frac{1}{2}\phi_m < \frac{1}{2}\pi$, which completes the proof.

Stability proof of $G_2(s)$. To prove that $G_2(s)$ is bounded in the open right half plane it is sufficient to show that the real part of $\alpha(s) - s$ is non-negative there. Defining the radii of $\alpha(s)$ and s by r_α and r, respectively, we need to show that $r_\alpha \cos\phi_\alpha \geqslant r\cos\phi$. Since $\alpha(s) = z_m/\sqrt{z_h}$ and $|z_m| > |z_h|$, it is clear that $r_\alpha > r$. Following the lines of the proof for $G_1(s)$, we have $\phi_m \leqslant 2\phi$. Therefore, $\frac{1}{2}\phi_m \leqslant \phi, \phi_\alpha \leqslant \phi$ and $\cos\phi_\alpha \geqslant \cos\phi$, which completes the proof.

Stability proof of $G_3(s)$. Since the damping ζ_h is always positive, the roots of $\widetilde{Z}(s)$ in (9) always lie in the open left half plane, implying that $|G_3(s)|$ is bounded in the open right half plane.

Stability proof of $G_4(s)$. Since we consider the principal surface of the complex plane leading to a non-negative real part of $\alpha(s)$, there are no solutions of $\alpha(s) = -s$ for s in the open right half plane. Therefore, there are no poles of $T(s)$ in the open right half plane, and it is thus bounded there. □

References

[1] N. Engheta, R.W. Ziolkowski, Metamaterials: Physics and Engineering Explorations, John Wiley & Sons, 2006.
[2] R. MarquÃ, F. MartÃn, M. Sorolla, et al, Metamaterials with negative parameters: theory, design, and microwave applications, vol. 183, John Wiley & Sons, 2011.
[3] C.M. Soukoulis, M. Wegener, Past achievements and future challenges in the development of three-dimensional photonic metamaterials, Nat. Photonics 5 (9) (2011) 523.

[4] D.R. Smith, D. Vier, N. Kroll, S. Schultz, Direct calculation of permeability and permittivity for a left-handed metamaterial, Appl. Phys. Lett. 77 (14) (2000) 2246–2248.
[5] M. Dubois, C. Shi, X. Zhu, Y. Wang, X. Zhang, Observation of acoustic dirac-like cone and double zero refractive index, Nature Commun. 8 (2017) 14871.
[6] C.A. Rohde, T.P. Martin, M.D. Guild, C.N. Layman, C.J. Naify, M. Nicholas, A.L. Thangawng, D.C. Calvo, G.J. Orris, Experimental demonstration of underwater acoustic scattering cancellation, Scientific Reports vol. 5 (2015), p. srep13175.
[7] F. Semperlotti, H. Zhu, Achieving selective interrogation and sub-wavelength resolution in thin plates with embedded metamaterial acoustic lenses, J. Appl. Phys. 116 (5) (2014) 054906 [Online].
[8] S.A. Cummer, D. Schurig, One path to acoustic cloaking, New J. Phys. 9 (3) (2007) 45.
[9] S.A. Cummer, J. Christensen, A. Alù, Controlling sound with acoustic metamaterials, Nature Rev. Mater. 1 (3) (2016) 16001.
[10] C. Caloz, T. Itoh, Electromagnetic Metamaterials: Transmission Line Theory and Microwave Applications, John Wiley & Sons, 2005.
[11] A. Lai, T. Itoh, C. Caloz, Composite right/left-handed transmission line metamaterials, IEEE Microwave Magazine 5 (3) (2004) 34–50.
[12] C. Caloz, T. Itoh, A. Rennings, CRLH metamaterial leaky-wave and resonant antennas, IEEE Antennas and Propag. Mag. 50 (5) (2008).
[13] N. Fang, D. Xi, J. Xu, M. Ambati, W. Srituravanich, C. Sun, X. Zhang, Ultrasonic metamaterials with negative modulus, Nature Mater. 5 (6) (2006) 452.
[14] C.J. Naify, C.N. Layman, T.P. Martin, M. Nicholas, D.C. Calvo, G.J. Orris, Experimental realization of a variable index transmission line metamaterial as an acoustic leaky-wave antenna, Appl. Phys. Lett. 102 (20) (2013) 203508.
[15] S.H. Lee, C.M. Park, Y.M. Seo, Z.G. Wang, C.K. Kim, Acoustic metamaterial with negative modulus, J. Phys.: Condens. Matter 21 (17) (2009) 175704.
[16] S.H. Lee, C.M. Park, Y.M. Seo, Z.G. Wang, C.K. Kim, Acoustic metamaterial with negative density, Phys. Lett. A 373 (48) (2009) 4464–4469.
[17] Y.M. Seo, J.J. Park, S.H. Lee, C.M. Park, C.K. Kim, S.H. Lee, Acoustic metamaterial exhibiting four different sign combinations of density and modulus, J. Appl. Phys. 111 (2) (2012) 023504.
[18] H. Huang, C. Sun, Wave attenuation mechanism in an acoustic metamaterial with negative effective mass density, New J. Phys. 11 (1) (2009) 013003.
[19] X.-N. Liu, G.-K. Hu, G.-L. Huang, C.-T. Sun, An elastic metamaterial with simultaneously negative mass density and bulk modulus, Appl. Phys. Lett. 98 (25) (2011) 251907.
[20] P.F. Pai, Metamaterial-based broadband elastic wave absorber, J. Intell. Mater. Syst. Struct. 21 (5) (2010) 517–528.
[21] H. Zhu, F. Semperlotti, Double-zero-index structural phononic waveguides, Phys. Rev. Appl. 8 (6) (2017) 064031.
[22] B.-I. Popa, D. Shinde, A. Konneker, S.A. Cummer, Active acoustic metamaterials reconfigurable in real time, Phys. Rev. B 91 (22) (2015) 220303.
[23] A.M. Baz, An active acoustic metamaterial with tunable effective density, J. Vib. Acoust. 132 (4) (2010) 041011.
[24] W. Akl, A. Baz, Multi-cell active acoustic metamaterial with programmable bulk modulus, J. Intell. Mater. Syst. Struct. 21 (5) (2010) 541–556.
[25] Y. Chen, G. Hu, G. Huang, A hybrid elastic metamaterial with negative mass density and tunable bending stiffness, J. Mech. Phys. Solids 105 (2017) 179–198.
[26] Y.-Z. Wang, F.-M. Li, Y.-S. Wang, Active feedback control of elastic wave metamaterials, J. Intell. Mater. Syst. Struct. 28 (15) (2017) 2110–2116.
[27] R. Curtain, K. Morris, Transfer functions of distributed parameter systems: a tutorial, Automatica 45 (5) (2009) 1101–1116.
[28] L. Sirota, A. Annaswamy, Modeling and control of wave propagation in a ring with applications to power grids, Provisionally accepted to IEEE Trans. Automatic Control, 2018.
[29] L. Sirota, Y. Halevi, Free response and absolute vibration suppression of second-order flexible structures–the traveling wave approach, J. Vib. Acoust. 132 (3) (2010) 031008.
[30] L. Sirota, Y. Halevi, Fractional order control of flexible structures governed by the damped wave equation, American Control Conference (ACC), 2015, IEEE, 2015, pp. 565–570.
[31] L. Sirota, Y. Halevi, Fractional order control of the two-dimensional wave equation, Automatica 59 (2015) 152–163.
[32] L. Sirota, A. Annaswamy, Active wave suppression in the interior of a one-domensional domain, Provisionally accepted to Automatica, 2018.
[33] L. Sirota, A.M. Annaswamy, Spatially continuous modeling and control of swing dynamics in electric power grids, IFAC-PapersOnLine 50 (1) (2017) 4400–4405.
[34] K.F. Graff, Wave Motion in Elastic Solids, Courier Corporation (2012).
[35] L. Sirota, Y. Halevi, The complete infinite series solution of systems governed by the wave equation with boundary damping, Wave Motion 51 (1) (2014) 114–124.
[36] L. Sirota, Y. Halevi, Extended d'alembert solution of finite length second order flexible structures with damped boundaries, Mech. Syst. Sig. Process. 39 (1–2) (2013) 47–58.
[37] B. Engquist, A. Majda, Radiation boundary conditions for acoustic and elastic wave calculations, Commun. Pure Appl. Math. 32 (3) (1979) 313–357.
[38] L. Sirota, Y. Halevi, Wave based vibration control of membranes, American Control Conference (ACC), 2014, IEEE, 2014, pp. 2729–2734.
[39] I. Liberal, N. Engheta, Near-zero refractive index photonics, Nat. Photonics 11 (3) (2017) 149–158.
[40] D. Matignon, Stability properties for generalized fractional differential systems, ESAIM: proceedings, vol. 5, EDP Sciences, 1998, pp. 145–158.